Desalination and Water Treatment
www.deswater.com

doi: 10.1080/19443994.2016.1173379

57 (2016) 22994–23006
October

Taylor & Francis
Taylor & Francis Group

Characterization of pressure retarded osmosis lab-scale systems

F. Giacalone, A. Cipollina, F. Grisafi, A. Tamburini*, G. Vella, G. Micale

Dipartimento di Ingegneria Chimica, Gestionale, Informatica, Meccanica (DICGIM), Università di Palermo (UNIPA) – viale delle Scienze Ed.6, 90128 Palermo, Italy, emails: francesco.giacalone07@unipa.it (F. Giacalone), andrea.cipollina@unipa.it (A. Cipollina), franco.grisafi@unipa.it (F. Grisafi), alessandro.tamburini@unipa.it (A. Tamburini), giuseppa.vella@unipa.it (G. Vella), giorgiod.maria.micale@unipa (G. Micale)

Received 24 June 2015; Accepted 23 February 2016

ABSTRACT

Power generation from salinity gradient is a viable alternative to produce energy from renewable sources. Pressure Retarded Osmosis (PRO) is one of the technologies proposed so far for the exploitation of such energy source. In the present preliminary work, two different geometry modules were tested under atmospheric pressure (i.e. forward osmosis or depressurized-PRO conditions). The first one is a conventional planar geometry cell. The second is a customized cylindrical membrane module, able to mechanically support the osmotic membrane along with the spacers. The latter, thanks to its design, allows membranes and spacers to be easily changed for testing purposes. A novel simplified procedure is proposed and employed in the planar geometry module to characterize an asymmetric membrane commercially available (i.e. assessing the water and salt permeability coefficients and the porous structure parameter). The parameters found were employed to mathematically estimate the permeate fluxes experimentally assessed and a very good agreement was found. Artificial solutions were employed for the experimental campaign: distilled water as feed solution and water–NaCl solution at different concentrations as drawing agent. Three different spacers were tested in the cylindrical geometry module thus highlighting the easy interchangeability of its components. Preliminary results confirmed that the spacer mesh open area is a critical issue affecting fluid dynamics (transport phenomena and pressure drop) along with membrane deformation.

Keywords: Salinity gradient power; PRO; Forward osmosis; Brine; Energy recovery

1. Introduction and literature review

New renewable forms of energy are needed, since fossil fuels have a number of drawbacks such as: emissions of greenhouse gases, depletion of finite sources, and dependence on a few oil-exporting regions in the world.

Wind power, hydropower, biofuel, solar power, geothermal power, and ocean power may be promising contributors to a sustainable development based on renewable energy.

*Corresponding author.

Presented at EuroMed 2015: Desalination for Clean Water and Energy Palermo, Italy, 10–14 May 2015. Organized by the European Desalination Society.

In this scenario, a significant potential to obtain clean energy is represented by the mixing of water streams with different salt concentrations. This salinity-gradient energy, also called blue energy, is available worldwide where fresh water streams flow into the sea. The global energy output from estuaries is estimated as 2.6 TW, which represents approximately 20% of the present worldwide energy demand.

These concepts were firstly reported in the literature many decades ago [1], but only in recent years the interest towards such renewable energy is spreading. The main technologies nowadays available to exploit salinity gradient energy are based on the use of suitable membranes: only in recent years membrane development has allowed their transport properties to be enhanced and their cost to be reduced thus leading the above technologies to become economically feasible. In particular, Reverse ElectroDialysis (RED) and Pressure Retarded Osmosis (PRO) are the mostly adopted and studied membrane-based processes for the conversion of salinity-gradient into usable energy [2,3]. RED makes use of ionic exchange membranes and red-ox reactions to directly convert salinity-gradient into electric energy [4–8]. The low concentration (i.e. low conductivity) typical of river water may be the main limit to the worldwide spreading of this technology [9–11]. In a PRO system, two solutions of different salinity are brought into contact by a semipermeable membrane. This membrane allows the solvent (i.e. water) to permeate and retains the solute (i.e. dissolved salts). The chemical potential difference between the solutions causes transport of water from the diluted salt solution to the more concentrated salt solution. If a hydrostatic pressure lower than the osmotic one is applied to the concentrated solution, the water transport will be partly retarded. The transport of water from the low-pressure diluted solution to the high-pressure concentrated solution results in a pressurization of the volume of transported water. This pressurized volume of transported water can be used to generate electrical power in a turbine [12–16].

The general equation describing the water transport across the membrane for any osmotic process (i.e. forward osmosis, PRO, or Reverse Osmosis) is the following:

$$J_w = A(\Delta\pi - \Delta P) \tag{1}$$

where J_w is the water flux passing through the membrane, A is the water-permeability of the membrane, $\Delta\pi$ is the osmotic pressure difference at membrane interfaces, and ΔP is the hydrostatic pressure difference between the two channels. The specific osmotic process occurring depends on the value of the hydrostatic pressure applied to the concentrated solution channel: $\Delta P = 0$ in forward osmosis, $\Delta P > \Delta\pi$ in reverse osmosis and $\Delta P < \Delta\pi$ in PRO.

The most important parameter regarding the PRO process is the power generated per unit membrane area (i.e. power density), which is clearly proportional to the water flux. In formulae:

$$W = J_w \Delta P = A(\Delta\pi - \Delta P)\Delta P \tag{2}$$

Different values of W can be obtained at different applied pressures (i.e. for $0 < \Delta P < \Delta\pi$). It can be demonstrated [16] that the maximum power is achieved when $\Delta P = \Delta\pi/2$:

$$W_{max} = A\left(\frac{\Delta\pi^2}{4}\right) \tag{3}$$

Asymmetric membranes where the skin layer is supported by a porous layer are usually employed in PRO unit in order to enhance membrane mechanical properties and withstand high pressure gradients. For this type of membranes, two different orientations are available: either active-layer front draw solution (AL-DS) or active layer front feed solution (AL-FS). According to previous studies in PRO applications [17], AL-DS orientation provides higher performance (better mechanical stability and higher permeate fluxes), although fouling effects may become more prominent [17].

When osmotic membranes are considered as not ideal, salt retro-diffusion from draw (concentrated) to feed (diluted) solution should be taken into account according to the following equation:

$$J_s = B(C_{d,m} - C_{f,m}) \tag{4}$$

where J_s is the salt flux through the membrane, B is the salt permeability of the membrane, $C_{d,m}$ is the salt concentration at the membrane-solution interface on the draw solution side, $C_{f,m}$ is the salt concentration at the membrane-solution interface on the feed solution side.

Water and salt fluxes through the membranes are responsible for another non-ideal phenomenon which is the concentration polarization (Fig. 1): when the fluid mixing is not sufficiently high, the water flux through the membrane towards the draw solution causes a reduction of the concentration at the membrane solution interface ($C_{d,m}$) with respect to the bulk ($C_{d,b}$). This phenomenon is named external

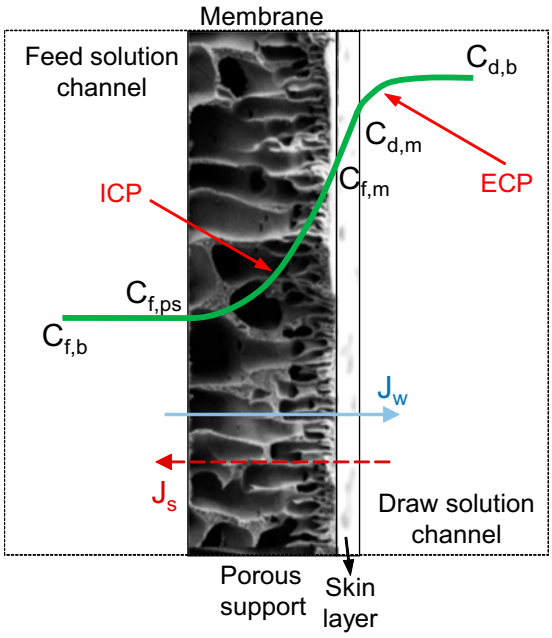

Fig. 1. An example of a concentration profile along with relevant polarizations in a PRO module section.

concentration polarization (ECP). Similarly, the combination of salt flux (towards the feed side) and water flux (towards the draw side) causes a concentration increase at the porous support-membrane skin layer interface ($C_{f,m}$) (where the fluid mixing is very poor) with respect to porous support-feed solution channel interface ($C_{f,ps}$): this concentration difference is called internal concentration polarization (ICP). When distilled water or river water are employed as feed solution, the concentration boundary layer within the feed solution channel, outside from the porous support is always much lower than ECP and ICP and is usually neglected (i.e. $C_{f,ps} \approx C_{f,b}$).

Clearly, both polarization phenomena and salt permeation contribute to decrease the concentration gradients on membrane interfaces (i.e. the driving force) thus resulting into a lower process performance.

The above-described polarizations ECP and ICP can be easily quantified by the following equations which can be obtained from mass balances on the corresponding layers reported in Fig. 1 [18,19]. For ECP:

$$C_{d,m} = C_{d,b}\exp\left(-\frac{J_w}{k}\right) - \frac{B}{J_w}(C_{d,m} - C_{f,m})\left[1 - \exp\left(-\frac{J_w}{k}\right)\right] \quad (5)$$

where k is the mass transfer coefficient in the draw solution channel.

As concerns ICP:

$$C_{f,m} = C_{f,b}\exp\left(\frac{J_w S}{D}\right) + \frac{B}{J_w}(C_{d,m} - C_{f,m})\left[\exp\left(\frac{J_w S}{D}\right) - 1\right] \quad (6)$$

where D is the salt diffusivity in water, S is the structure parameter of the porous support layer defined as $S = s\tau/\varepsilon$ (where s is porous medium thickness, τ is tortuosity and ε is porosity). Notably, the concentration can be easily transformed into osmotic pressure via the well-known Van't Hoff equation ($\pi = iCRT$, where R is the ideal gas constant, T is temperature, i is the Van't Hoff coefficient equal to 2 for NaCl).

By accounting for these non-ideal phenomena (polarization and salt permeation), the corresponding water flux can be expressed as:

$$J_{w,real} = A\left\{\frac{\pi_{d,b}\exp\left(-\frac{J_w}{k}\right) - \pi_{f,b}\exp\left(\frac{J_w S}{D}\right)}{1 + \frac{B}{J_w}\left[\exp\left(\frac{J_w S}{D}\right) - \exp\left(-\frac{J_w}{k}\right)\right]} - \Delta P\right\} \quad (7)$$

where $\pi_{d,b}$ and $\pi_{f,b}$ are the osmotic pressures in the bulk of the draw and of the feed solution channel, respectively.

Depending on the operating conditions of a real PRO module, other effects may be crucial and very detrimental for the process outcome: fouling and membrane deformation are the most important.

Fouling is the deposition of substances contained in the feed stream at the membrane surface or inside the pores. The interaction between the foulants and the membrane surface reduces the membrane water flux, in some cases the fouling can chemically degrade the membrane material and consequently influences the economics of the operation [20]. The mechanism of fouling is complex and depends of many factors such as water quality, temperature, system design, cleaning, water flow, membrane surface, etc. These factors need to be properly accounted for in process design and development to mitigate fouling. Fouling in osmotically driven membrane process is different from fouling in pressure-driven membrane processes since the deposition of foulant occurs on different membranes surfaces depending on the membrane orientation. In FO mode foulant deposition occurs on the smooth active layer, in PRO mode foulant deposition takes place on the rough support layer side, or even within the support layer [21], thus leading the fouling effect to be more marked [17]. Membrane deformation is a critical aspect, which should be taken into full account in PRO operation: given the applied pressure

difference between the diluted and the concentrated channel, the membrane can exhibit a deep deformation. In this regard, the geometry of the spacer is crucial, since a different mesh opening area could leads to very different membrane deformation and subsequent process performance [22,23].

In accordance with the equations reported above, asymmetric osmotic membranes are characterized by three different coefficients: water permeability A, salt permeability B and structure parameter of the porous support S. For a given membrane, these three parameters can be assessed by following a standard methodology reported in the literature [24,25]. Following this methodology, three different tests have to be carried out: two in reverse-osmosis operation mode, the third in forward-osmosis. The first test in RO mode is performed with distilled water to assess coefficient A, the second test makes use of a salty solution (under the same operating conditions) to obtain the membrane salt rejection factor r:

$$r = 1 - \frac{C_{\text{permeate}}}{C_{\text{feed}}} \tag{8}$$

Coefficient B can be inferred from this factor via the following Eq. (9):

$$B = J_{\text{w}}\left(\frac{1-r}{r}\right)\exp\left(-\frac{J_{\text{w}}}{k}\right) \tag{9}$$

where k is the mass transfer coefficient. The last test, carried out in FO mode employs a 1 M water solution as the concentrated solution and distilled water as the diluted solution. On the basis of the water flux measured, the parameter S can be assessed according to the following correlation valid for the AL-FS configuration (active layer facing the feed solution) [18]:

$$S = \frac{D}{J_{\text{w}}}\ln\left(\frac{B + A\pi_{\text{d,b}}}{B + J_{\text{w}} + A\pi_{\text{f,b}}}\right) \tag{10}$$

Notably, Eq. (10) is derived by neglecting ECP (i.e. only ICP is taken into account, that is $\pi_{\text{f,m}} = \pi_{\text{f,b}}$).

In recent years, many efforts have been devoted to the study of PRO focusing (i) on the production of membranes able to exhibit high water fluxes and mechanical resistance and (ii) on the proposition of a novel geometry being reliable at the industrial scale. In this regard, Straub et al. [26] have recently proposed an innovative planar geometry module: it is a specially designed cross flow test cell able to allow PRO operation at very high applied hydraulic pressures. This geometry was found able to resist up to 48 bar of applied pressure on the draw solution channel. Kim et al. [27] investigated the performance of a spiral wound module provided with a woven tricot spacer in PRO conditions: such spacer was found to have a detrimental impact on the process performance. For a 0.6 M NaCl solution and tap water, they achieved a maximum power density of 1.0 W/m^2 at a hydraulic pressure difference of 9.8 bar. Chou et al. [28] developed a TFC hollow fiber membrane module fed by artificial (i.e. NaCl-water) solutions (1.0 M draw solution and 1 mM feed solution). For this system, authors report (i) reverse salt fluxes much lower than those in flat-sheet membranes; (ii) and achievable power density of 20.9 W/m^2 at a pressure of 15 bar.

Membrane characterization is usually performed in small planar geometry units (membrane area of about 100 cm^2), which are also employed to test different spacers and/or configurations. However, such a geometry is expected to be different from those that may be suitable at an industrial scale. In addition, testing different spacers/configuration for the case of standard spiral wound modules would require assembling a different module for each case to be tested. In this regard, the aim of this preliminary work is to propose an up-scaling of a module for laboratory experimental testing through a novel cylindrical geometry system allowing membrane characterization and spacer-channel investigation to be performed in a geometry more similar to the industrial one. This novel system (as typical planar geometry modules) can be assembled and disassembled in order to guarantee an easy interchangeability of its components (e.g. spacer and membrane) and would allow an easier analysis of the fluid dynamics within the channels.

Summarizing, in the first part of the present work, a preliminary characterization of the membrane employed through a novel simplified procedure proposed here is presented: the parameters obtained are employed to calculate the permeate fluxes and compare them with the ones experimentally measured. In the second part, the novel cylindrical system is presented and some preliminary results are shown.

2. Experimental

2.1. Planar geometry system

In the first part of this work a lab-scale planar system is designed and built (i) to characterize a commercial osmotic membrane (HTI OsMem™ TFC-ES membrane) and (ii) to assess its performance at various osmotic pressure differences. This system presents the asymmetric-membrane orientation typical of PRO

modules (i.e. AL-DS) but it is operated without pressurizing the draw solution channel (ΔP of Eq. (1) equal to zero). Such AL-DS membrane orientation along with applied $\Delta P = 0$ is known as the so called "Unpressurized" retarded osmosis condition [29].

The experimental apparatus is constituted of two-squared polycarbonate plates with equal sides 20 and 5 cm thickness (Fig. 2). The two plates are provided with three inlet channels and three outlet channels for each side. These aid the flow distribution within the module. The feed and draw solution are forced by two peristaltic pumps (verderflex M025 peristaltic pump) to move through the inlets within two channels (one for the concentrated solution, the other for the diluted) provided with the same diamond woven spacer (supplied by Deukum GmbH). This spacer is 270 μm thick, has a mesh opening of 600 μm and a wire diameter of 150 μm. The corresponding hydraulic diameter and shadow factor (open area/total area of a single mash) were estimated to be equal to 300 μm and 0.67, respectively. An asymmetric osmotic membrane (HTI OsMem™ TFC-ES Membrane) is interposed between the two spacer-filled channels: the orientation was AL-DS in accordance with the literature [17]. The sealing of the system is guaranteed by through screws and bolts tightened by a torque wrench.

The test rig (Fig. 3) allows a double measurement of the permeate flow: (i) as concerns the concentrated solution, a scale is employed to determine the variations in time of the weight; (ii) correspondingly, two graduated tanks are employed to measure the variation in time of the volume of the diluted solution.

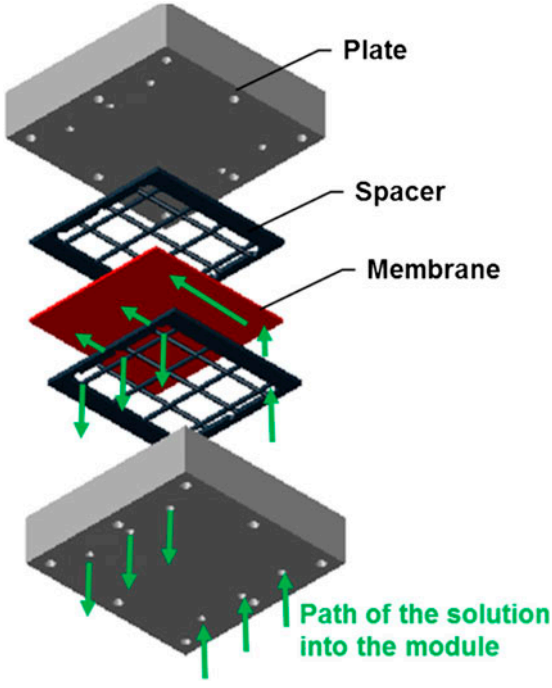

Fig. 2. Sketch of the planar geometry module.

More precisely, the tank with the in-concentrated solution and the tank with the out-concentrated solution are placed upon a scale and their weight is monitored during time. The flux is calculated by dividing the difference between the initial and the final weight by the elapsed time and the effective membrane area (membrane area times the spacer shadow factor). An analogous methodology was employed for the diluted solution: the tank with the in-diluted solution and the one with the out-diluted solution were graduated thus allowing the total volume of diluted solution to be monitored over time. The permeate flux was estimated by dividing the difference of the initial and final solution volume by the product of elapsed time times the effective membrane area. Clearly, the second measurement is employed in order to recognize possible leakages outgoing from the test rig: a measurement on a single channel is not sufficient to distinguish external leakages from permeate flux. When leakages do not occur, the two measurements provide identical values (discrepancies up to ~2% were found). An example of the data obtained during the test is reported in Fig. 4: distilled water as diluted solution and 0.6 M NaCl-water solution as the concentrated one. Clearly, the slope of the two data-sets indicates the permeate flow rate through the membrane.

The conductivity is monitored with a conductivity meter and the pressure drops are measured by means of two manometers connected to the two inlets (concentrated solution and diluted solution inlets) of the module.

Experiments were carried out both using NaCl-water solutions (i.e. "artificial" solutions). "Artificial" solutions tests were performed by employing distilled water (0.4 mM corresponding to a conductivity of 40 μScm) as the diluted solution and NaCl-water solutions at different concentrations (ranging from 0.1 to 1 M corresponding to a conductivity of 10.6 and 85.7 mS/cm respectively) as the concentrate. The draw solution concentrations investigated encompass $\Delta\pi$ different from the typical obtainable for the couple river water-seawater. Experiments were carried out at ambient temperature (~20˚C) and at fixed flow rate equal to 82 ml/min for both solutions (feed and draw).

2.2. Cylindrical geometry system

As reported above, a novel cylindrical geometry system being an upscaling of the standard planar

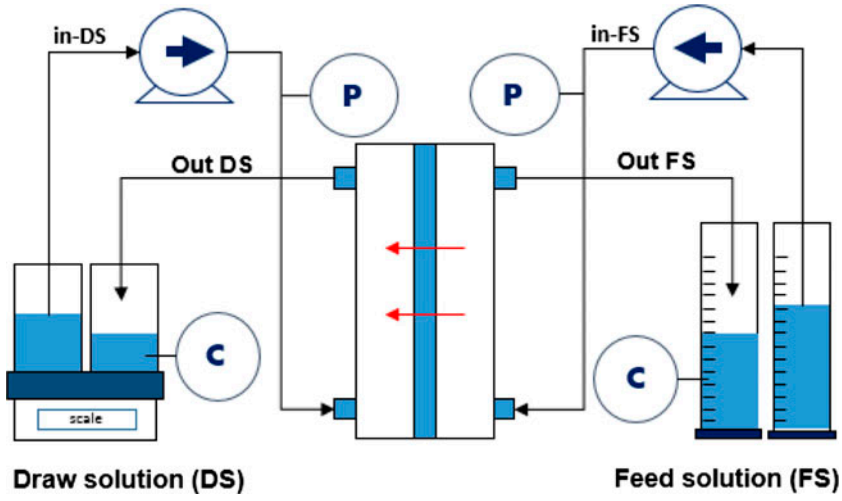

Fig. 3. Test rig for the planar geometry system.

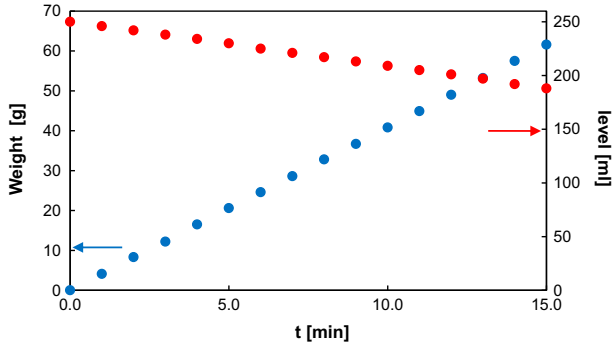

Fig. 4. Example of the data collected during the experiments: liquid level (in and out diluted solutions) and liquid weight (in and out diluted solutions) as a function of time. Feed solution: distilled water, Q_f = 82 ml/min; draw solution: NaCl-water, Q_d = 82 ml/min, $C_{d,b}^{in}$ = 0.6 M.

geometry one is proposed. Such novel geometry would allow the possibility of easily testing different spacer-configurations, a feature typical of planar geometry modules. At the same time, it is more similar to large-scale modules where the cylindrical geometry guarantees a better seal at large pressure gradients (typical of PRO operations). Notably, when seawater and river water are employed in a PRO unit, an osmotic pressure difference of about 30 bar is encountered. In order to maximize the power output, the difference of hydraulic pressure should be imposed at 15 bar. The membrane should be properly supported in order to resist at these conditions. Moreover, the module should be able to stand such pressure difference values without exhibiting any leakage. Since saline solutions are employed, plastic materials (Nylon) were employed to avoid any corrosion issue.

The proposed geometry is composed of two different elements (Fig. 5): a nylon cylindrical support for the membrane and a tube with a larger diameter able to host the support. More precisely, the spacer to be tested is wound around the external surface of the cylinder, the membrane is wound around the spacer in the same way. The sealing is guaranteed by a small aluminium plate, which is tightened to the cylinder by screws. This cylinder-spacer-membrane assembly constituting the feed solution channel is inserted within a tube, and the resulting annulus constitutes the draw solution channel (Fig. 5). Cylindrical o-ring gaskets allow the sealing with the outer tube. The module was designed in order to effectively withstand pressures of 15 bar.

The feed solution enters within the inner tube and through some radial holes is distributed along the external surface of the cylinder within the spacer-filled channel. Conversely, the draw solution is forced to move within the annulus between the membrane and the outer tube. Of course, the membrane is placed with the AL-DS orientation. The present module configuration was thought to reduce the membrane deformation effects and reduce leakages risks under PRO conditions. Moreover, it is very easy to change the spacer and/or the membrane to test different configurations. As shown in Fig. 5, the module was operated under co-current mode, although counter-current operation mode is also possible.

The test rig is practically the same reported in Fig. 3 for the planar geometry module. In this case, a rotary vane pump is employed to let the draw solution circulation. The experimental procedure is also the same. Given the preliminary nature of the present

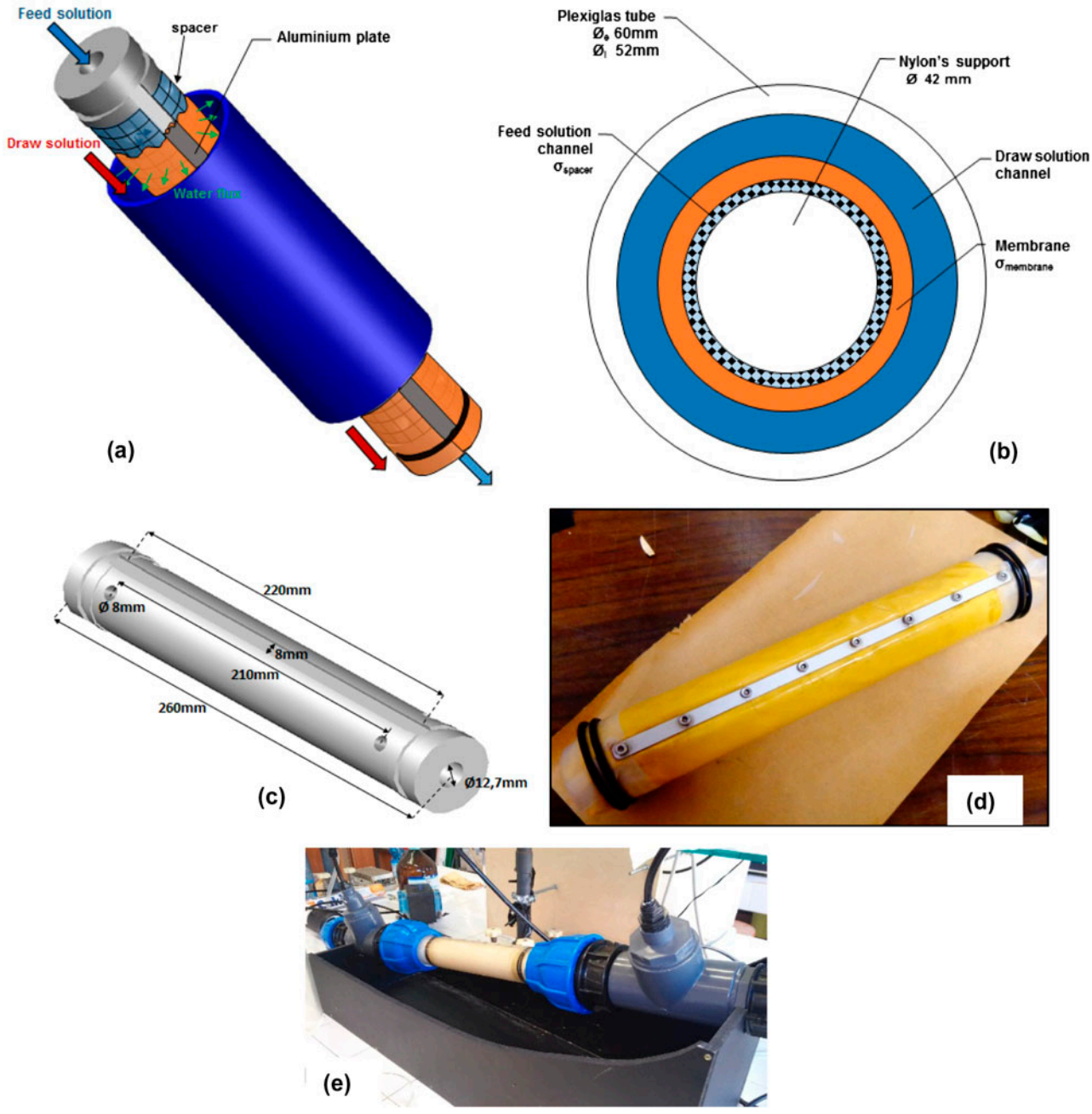

Fig. 5. Sketches and photos of the cylindrical geometry module: (a) module assembly and operation, (b) detail of the module layers, (c) nylon support, (d) membrane installation (aluminium plate and o-ring are shown), and (e) whole module after assembly.

work, only tests under unpressurized retarded osmosis conditions were conducted with this novel geometry: the permeate flux was assessed at different draw solution concentrations. The effect of different spacers in the feed solution channel on the permeate flux was addressed: in particular three different commercial spacers were tested (Fig. 6). Notably, for these preliminary tests no spacer was inserted in the draw solution channel.

The features of these spacers are summarized in Table 1.

For each spacer, tests concern the estimate of the permeate fluxes obtained with distilled water as feed solution and a NaCl-water solution at different

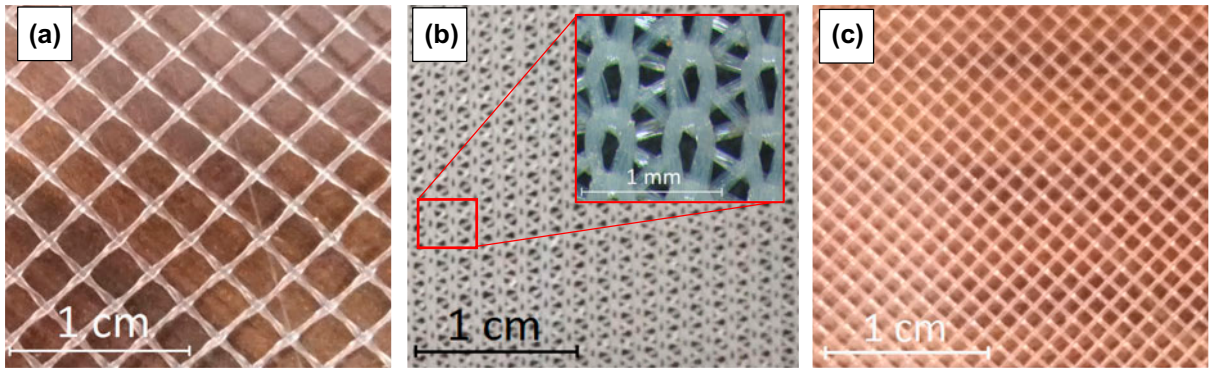

Fig. 6. Tested spacers: (a) Spacer A, (b) Spacer B, and (c) Spacer C.

Table 1
Investigated spacers

Spacer code	Spacer thickness (μm)	Wire diameter (μm)	Wire configuration	Wire angle	Flow attach angle[a]	Additional wire features	Shadow factor (%)
Spacer A	620	320	Overlapped	90°	45°	Hard and stiff	0.74
Spacer B	220	–	Woven	Variable	Variable	Soft	Very high
Spacer C	490	250	Overlapped	90°	45°	Slightly stiff	0.58

[a]Angle between the main flow direction and spacer wires.

concentrations (ranging from 0.1 to 1 M) as draw agent. The feed flow rate was fixed at 5.52 l/h in all cases. The membrane area available which is used for the permeate flux calculation from the weight measurements was equal to 0.023 m^2 (0.2 × 0.115 m). Spacer shadow factors are reported in Table 1. Notably, due to its intrinsic irregularity, it was not possible to assess some features of the spacer B (Table 1).

It is worth noting that the spacer comparison has been performed only in order to evaluate their suitability for our specific cylindrical configuration, rather than thoroughly evaluate the effect of mesh and opening size on membrane deformation and process performance (as already done by other authors [22,23]).

3. Results and discussion

3.1. Planar geometry module

The planar geometry module was employed to characterize the membrane and to analyze its performance with a number of different salinity gradients (i.e. different $\Delta\pi$).

3.1.1. Membrane characterization

Membrane characterization requires the assessment of the membrane main parameters: A, B, and S. For the present case, a simplified procedure was employed for the membrane characterization. Unpressurized retarded osmosis ($\Delta P = 0$) conditions were adopted for this purpose. Under these conditions and when non-ideal phenomena (i.e. salt permeation and concentration polarizations) are negligible ("ideal flux"), water flux is directly proportional to osmotic pressure difference at the membrane interfaces ($J_w = A \cdot \Delta\pi$). Otherwise, the relation between water flux and driving force is not linear ("real flux", see Eq. (7)). The experimentally obtained J_w vs. $\Delta\pi$ trend is reported in Fig. 7.

A close inspection of this trend shows this non-linear behaviour only at medium to large values of the driving force, while the relation is linear at very low values of $\Delta\pi$. This behaviour at low $\Delta\pi$ is better shown in Fig. 8. Such experimental finding is not surprising since non-ideal phenomena as concentration polarization depend on the driving force thus becoming more significant only when high permeate fluxes occur. Therefore, at very low driving force non-ideal phenomena are so low that can be reasonably neglected. Under these conditions, the water permeability coefficient A can be easily assessed as the slope of the J_w vs. $\Delta\pi$ trend and was estimated to be ~2 l/m^2 hbar. Notably, the error bars reported in Fig. 8 are relevant to the scale measurement uncertainty that was estimated to be 0.05 g.

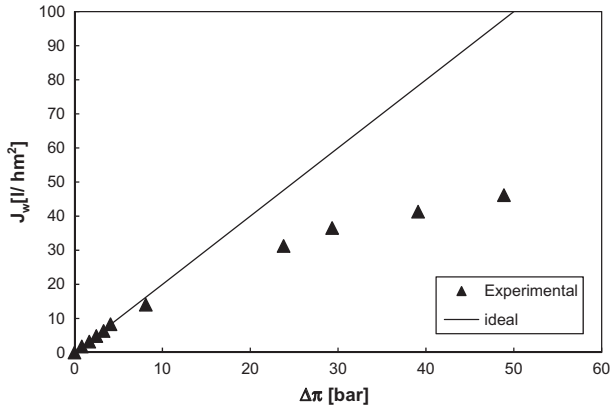

Fig. 7. Real and ideal water flux as a function of osmotic pressure difference.

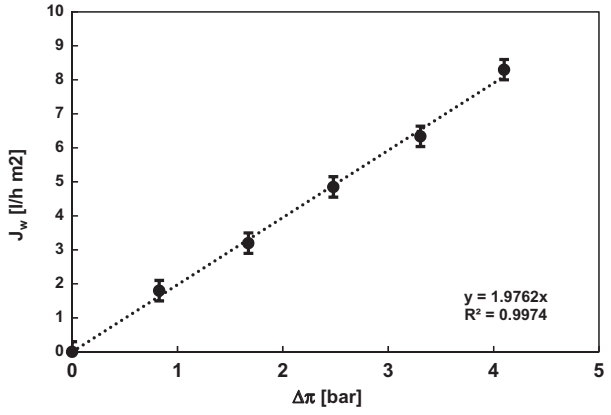

Fig. 8. Permeate flux vs. $\Delta\pi$ at low $\Delta\pi$.

For the assessment of parameters B and S, a procedure combining an experimental and a mathematical approach was employed. In particular, it is well known that B and S are related to the aforementioned Eq. (10) which for the case of AL-DS membrane orientation modifies as in the following:

$$S = \frac{D}{J_w} \ln\left(\frac{B + A\overline{\pi_{d,b}} - J_w}{B + A\overline{\pi_{f,b}}}\right) \tag{11}$$

As already mentioned for Eq. (10), ECP is not taken into account. The experiments carried out in this work including those employed for the assessment of B and S (draw solution concentrations of 0.6, 0.8 and 1 M) were carried out at a flow rate being so high that very low ECP were expected (a-posteriori calculations provided ECP lower than 7% of the total $C_{d,b} - C_{f,b}$). As a first step of the procedure, a value of B was preliminarily and arbitrarily fixed; then, for each experiment "i", a corresponding S_i value was calculated via Eq. (11). Notably, an average concentration between inlet and outlet was used for the calculation. Once "n" experiments were carried out, a mean S value (S_{av}) and the corresponding variation coefficient VC were calculated:

$$S_{av} = \sum_{i=1}^{n} S_i \tag{12}$$

$$VC = \frac{1}{S_{av}} \sqrt{\sum_{i=1}^{n} \frac{(S_i - S_{av})^2}{n}} \tag{13}$$

Then, a different B value was tested and a corresponding different VC was calculated and so on (B was letting to vary in a large range). Clearly, the right value of B is the one guaranteeing that Eq. (11) provides the same S value for each flux measured (i.e. each experiment). Therefore, B was chosen as that corresponding to the lowest value of VC. Once B was assessed, S was chosen as the corresponding S_{av}. The trend of the VCs calculated as a function of B is reported in Fig. 9. As it can be seen, the final B value was 2.70×10^{-7} m/s, the corresponding S was 463 μm. These values are in accordance with others found in the literature for similar membranes [24,26].

The main advantage of the membrane characterization method proposed with respect to the ones available in the literature [22–24] is the possibility of getting membrane properties using FO-tests, (i) which does not need to carry out experiments under pressurized conditions, and (ii) where membrane is kept with the same orientation (AL-DS) of the PRO operation mode. Of course, the soundness of the method should be validated in the future by comparing the membrane parameters obtained with those provided by other well-known methods available in the literature.

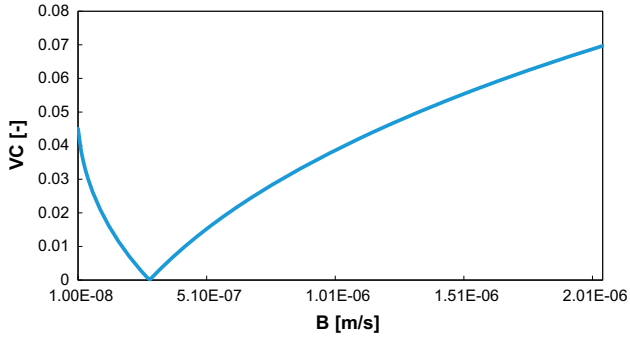

Fig. 9. Variation coefficient VC as a function of the arbitrarily tested B.

3.1.2. Comparison between experimental and calculated permeate fluxes

Once the membrane parameters have been evaluated, the permeate fluxes could be mathematically estimated by Eq. (7). The use of this equation requires the preliminary estimate of the mass transfer coefficient k (necessary to evaluate ECP) which was derived from data available in the literature for woven spacers. The flow rate of the draw solution corresponds to a void Reynolds number [30–34] $Re \approx 24.6$, the physical properties correspond to a Schmidt Number $Sc \approx 666$. For this pair of Re and Sc, a void Sherwood number $Sh \approx 50$ was found in the literature [33]. The corresponding k value was equal to $\sim 1.39 \times 10^{-4}$ m/s. The following Fig. 10 shows the comparison between experimental and the calculated permeate fluxes: as it can be observed, the calculated fluxes are in very good agreement with the experimental ones, thus somehow confirming the goodness of the procedure employed to assess the membrane parameters.

3.2. Cylindrical geometry module

As anticipated in Section 2.2, preliminary experiments were carried out with the cylindrical module under unpressurized retarded osmosis conditions: in particular the effect of the feed solution channel-spacer along with the draw solution concentration on the process performance was evaluated.

3.2.1. Spacer A

This commercial spacer is employed in feed channels of spiral wound modules for reverse osmosis. It has the highest mesh size (among the spacers investigated here), thus, it is expected to exhibit the lowest shadow effect and the lowest pressure drop. On the other hand, high deformation rate of the membrane is also expected.

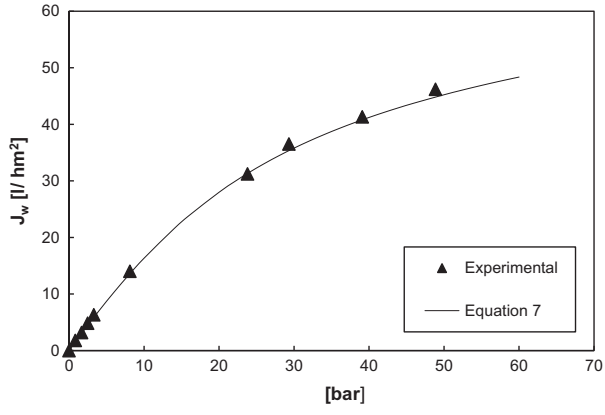

Fig. 10. Comparison between experimental and calculated (Eq. (7)) permeate fluxes.

This specific spacer was found to be unsuitable for this novel geometry module: the wires are too hard and stiff to be correctly wound around the nylon cylinder. In particular, the module is however assembled, but some internal leakages were recognized (irregular weight vs. time trend) thus resulting into unreliable measurements. Also, at the end of the tests the membrane was found to be highly deformed and even pierced in some points because of the stiff edges (critical spacer-membrane contact points) exhibited by this spacer. Notably, RO membranes are much thicker than those employed in this work and do not suffer from the presence of these stiff edges.

3.2.2. Spacer B and C

Spacer B is usually employed in the permeate channel of spiral wound reverse osmosis modules. It is softer than spacer A, it has no stiff edges and a very low mesh size. No internal leakages occurred and reliable permeate flux estimates were obtained. Spacer C was supplied by Deukum and exhibits a shadow factor similar to the spacer employed for the planar geometry module tests. Also spacer C showed features compatible with the module assembly and reliable estimates were possible. Relevant results are reported in Fig. 11.

As it can be seen, in all cases the J_w vs. $\Delta\pi$ trend is not linear and comparable with that relevant to the planar geometry system: also in this case, as the driving force increases, non-ideal detrimental phenomena increase as well. In particular, in the cylindrical module the draw solution channel is unprovided with a spacer, thus resulting into significant polarization phenomena (i.e. ECP). As concerns the comparison between the two spacers, Fig. 11 shows that larger permeate fluxes can be obtained with spacer C. The two spacers are placed in the feed solution channel where ECP is usually negligible; therefore, the different performance is allegedly due to the very different mesh opening area: the shadow effect exhibited by spacer B is largely higher than that of spacer C. For the case of spacer C two tests at different draw solution flow rates were performed: Fig. 11 shows that higher fluxes are achieved at a higher flow rate (350 l/h). Since no spacers are present in the draw solution side, this enhancement of the flux, due to velocity components perpendicular to the membrane [31], might be generated either by the radial inlets or by the onset of turbulent conditions. Otherwise, if

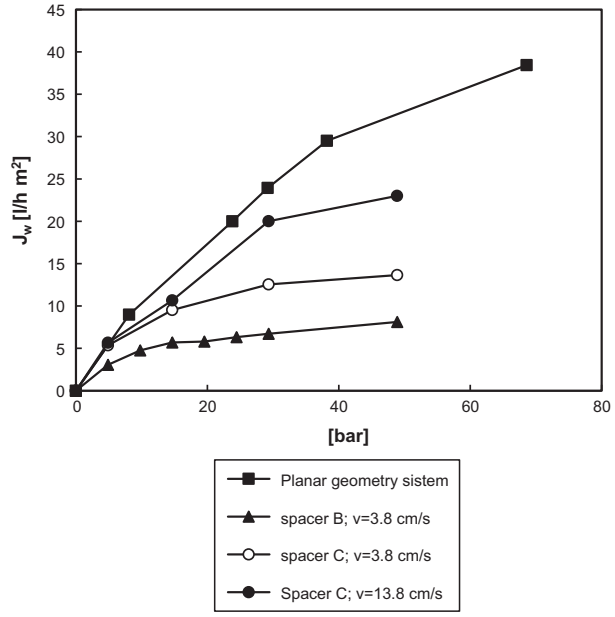

Fig. 11. Comparison of the permeate flux vs. osmotic pressure trends: effects of feed solution channel spacer, draw solution flow rate and geometry module. The features of the spacer A, B, C used in the cylindrical module are reported in the Table 1. The planar geometry system data reported for a purely qualitative comparison are obtained with a diamond woven spacer (supplied by Deukum GmbH) 270 μm thick, with mesh opening of 600 μm and wire diameter of 150 μm).

laminar conditions were present, no effect would be observable. Fig. 11 reports also a purely qualitative comparison with the flux obtained in the planar geometry system. As it can be seen, when the osmotic pressure difference is lower than 15 bar, the two modules provides similar fluxes, while at larger $\Delta\pi$, the higher $\Delta\pi$, the larger their disagreement. This is allegedly due again to the high ECP exhibited by the cylindrical module on the draw solution side, the ECP increases as the permeate flux increases. Of course, it should be kept in mind that such comparison is purely qualitative since the modules are characterized by many differences: slightly different spacers (the planar geometry one exhibits a lower shadow factor), different operating conditions (i.e. Reynolds number).

4. Conclusions and future remarks

In the present preliminary work, an experimental analysis was performed within two different membrane modules which were tested under unpressurized retarded osmosis conditions.

In particular, the first module is a conventional planar geometry cell. It was used to characterize a commercial asymmetric membrane provided by HTI™. A novel simplified procedure is proposed and employed for this purpose: it takes advantage from permeate flux measurements at different osmotic gradients to assess the membrane water permeability *A*; conversely, a numerical procedure is adopted to assess the membrane salt permeability *B* and the membrane structure parameter *S*. The parameters found were employed to mathematically estimate the permeate fluxes experimentally assessed and a very good agreement was found. However, this simplified procedure for membrane characterization should be in the future validated also with data obtained via the standard procedure employed in the literature [24,25]. For all experiments, artificial solutions were employed: distilled water as feed solution and NaCl-water solution as draw agent. In particular, different saline concentrations were tested and corresponding permeate fluxes were assessed. Results indicated that polarization phenomena could become prominent at high osmotic gradients (i.e. large permeate fluxes).

The second module employed in the present work is a novel cylindrical geometry system purposely designed, constructed and tested. It has a scale larger than that typical of the planar geometry systems usually employed for laboratory investigations and it is an assembly allowing different spacers and/or membranes to be easily tested. For this geometry, three different commercial spacers were tested. Results suggest that spacers with too stiff wires are not suitable to be employed in this system. Results also confirm that the spacer mesh open area is a critical parameter affecting the permeate flux through (i) the shadow factor effect and (ii) the membrane deformation extent. In the future, this novel geometry will be tested under the application of a pressure difference between the two channels in order to find the most suitable spacer-membrane configuration able to deal with non-conventional salinity gradients: just as an example, brine deriving from desalination plants and saltworks (easily available) in Sicily (Italy) will be employed for the experimental campaign.

Acknowledgements

This work was carried out under financial support (i) by the Italian ''Ministero dell'Istruzione, dell'Università e della Ricerca'', P.R.I.N. 2010-11 "Hydroelectric Energy by Pressure Retarded Osmosis in Coastal Areas" contract n° 2006091953_004 and (ii) by the European project "STAGE-STE" (Grant Agreement no. 609837).

Nomenclature

Symbols

A	—	membrane water permeability coefficient (m s^{-1} bar^{-1})
B	—	membrane salt permeability coefficient (m s^{-1})
C	—	salt concentration (mol m^{-3})
D	—	diffusivity (m^2 s^{-1})
H	—	channel height (m)
i	—	Van't Hoff coefficient (–)
J_s	—	salt flux (mol m^{-2} s^{-1})
J_w	—	water flux (l m^{-2} h^{-1})
k	—	mass transfer coefficient (m s^{-1})
l	—	mesh length (m)
Q	—	flow rate (m^3/s)
r	—	salt rejection factor (–)
R	—	ideal Gas constant (bar l mol^{-1} K^{-1})
Re	—	Reynolds number v·2h/v (–)
s	—	porous medium thickness (m)
S	—	membrane structure parameter (m)
Sc	—	Schmidt number v/D (–)
Sh	—	Sherwood number k 2h/v (–)
T	—	temperature (K)
v	—	velocity (void velocity => flow rate divided passage section) (m s^{-1})

Greek symbols

ε	—	porous medium porosity (–)
μ	—	dynamic viscosity (Pa s)
ν	—	kinematic viscosity (μ/ρ m^2 s^{-1})
π	—	osmotic pressure (bar)
ρ	—	density (Kg m^{-3})
σ	—	thickness (m)
τ	—	porous medium tortuosity (–)

Subscripts

b	—	bulk
d	—	draw
f	—	feed
high	—	concentrated
low	—	diluted
m	—	solution-membrane interface
ps	—	porous support
s	—	salt
w	—	water

Superscripts

in	—	solution entering the module
out	—	solution outgoing from the module

Average

$\bar{\Phi}$	—	in-out average of the generic quantity Φ

References

[1] R.E. Pattle, Production of electric power by mixing fresh and salt water in the hydroelectric pile, Nature 174 (1954) 660.

[2] N.Y. Yip, M. Elimelech, Comparison of energy efficiency and power density in pressure retarded osmosis and reverse electrodialysis, Environ. Sci. Technol. 48 (2014) 11002–11012.

[3] F. Helfer, C. Lemckert, Y.G. Anissimov, Osmotic power with pressure retarded osmosis: Theory, performance and trends—A review, J. Membr. Sci. 453 (2014) 337–358.

[4] K. Nijmeijer, S. Metz, Salinity gradient energy, Sustainability Sci. Eng. 2 (C) (2010) 95–139.

[5] O. Scialdone, A. D'Angelo, A. Galia, Energy generation and abatement of Acid Orange 7 in reverse electrodialysis cells using salinity gradients, J. Electroanal. Chem. 738 (2015) 61–68.

[6] D.A. Vermaas, J. Veerman, M. Saakes, K. Nijmeijer, Influence of multivalent ions on renewable energy generation in reverse electrodialysis, Energy Environ. Sci. 7 (2014) 1434–1445.

[7] A. Tamburini, G. La Barbera, A. Cipollina, M. Ciofalo, G. Micale, CFD simulation of channels for direct and reverse electrodialysis, Desalin. Water Treat. 48 (2012) 370–389.

[8] A. Tamburini, G. La Barbera, A. Cipollina, G. Micale, M. Ciofalo, CFD prediction of scalar transport in thin channels for reverse electrodialysis, Desalin. Water Treat. 55(12) (2015) 3424–3445.

[9] M. Tedesco, A. Cipollina, A. Tamburini, W. van Baak, G. Micale, Modelling the reverse electrodialysis process with seawater and concentrated brines, Desalin. Water Treat. 49 (2012) 404–424.

[10] M. Tedesco, A. Cipollina, A. Tamburini, I.D.L. Bogle, G. Micale, A simulation tool for analysis and design of reverse electrodialysis using concentrated brines, Chem. Eng. Res. Des. 93 (2015) 441–456.

[11] M. Tedesco, A. Cipollina, A. Tamburini, G. Micale, J. Helsen, M. Papapetrou, REA Power: Use of desalination brine for power production through reverse electrodialysis, Desalin. Water Treat. 53 (2015) 3161–3169.

[12] A. Achilli, A.E. Childress, Pressure retarded osmosis: From the vision of Sidney Loeb to the first prototype installation—Review, Desalination 261 (2010) 205–211.

[13] J. Maisonneuve, P. Pillay, C.B. Laflamme, Pressure-retarded osmotic power system model considering non-ideal effects, Renewable Energy 75 (2015) 416–424.

[14] A. Yaroshchuk, Optimal hydrostatic counter-pressure in pressure-retarded osmosis with composite/asymmetric membranes, J. Membr. Sci. 477 (2015) 157–160.

[15] A. Altaee, G. Zaragoza, A. Sharif, Pressure retarded osmosis for power generation and seawater desalination: Performance analysis, Desalination 344 (2014) 108–115.

[16] A. Achilli, T.Y. Cath, A.E. Childress, Power generation with pressure retarded osmosis: An experimental and theoretical investigation, J. Membr. Sci. 343 (2009) 42–52.

[17] Q. She, X. Jin, C.Y. Tang, Osmotic power production from salinity gradient resource by pressure-retarded osmosis: Effects of operating conditions and reverse solute diffusion, J. Membr. Sci. 401–402 (2012) 262–273.

[18] S. Loeb, L. Titelman, E. Korngold, J. Freiman, Effect of porous support fabric on osmosis through a Loeb-Sourirajan type asymmetric membrane, J. Membr. Sci. 129 (1997) 243–249.

[19] N.Y. Yip, A. Tiraferri, W.A. Phillip, J.D. Schiffman, L.A. Hoover, Y.C. Kim, M. Elimelech, Thin-film composite pressure retarded osmosis membranes for

sustainable power generation from salinity gradients, Environ. Sci. Technol. 45 (2011) 4360–4369.
[20] D. Rana, T. Matsuura, Surface modifications for antifouling membranes, Chem. Rev. 110 (2010) 2448–2471.
[21] A. Seidel, M. Elimelech, Coupling between chemical and physical interactions in natural organic matter (NOM) fouling of nanofiltration membranes: Implications for fouling control, J. Membr. Sci. 203 (2002) 243–255.
[22] Y.C. Kim, M. Elimelech, Adverse impact of feed channel spacers on the performance of pressure retarded osmosis, Environ. Sci. Technol. 46(8) (2012) 4673–4681.
[23] Q. She, D. Hou, J. Liu, K.H. Tan, C.Y. Tang, Effect of feed spacer induced membrane deformation on the performance of pressure retarded osmosis (PRO): Implications for PRO process operation, J. Membr. Sci. 445 (2013) 170–182.
[24] T.Y. Cath, M. Elimelech, J.R. McCutcheon, R.L. McGinnis, A. Achilli, D. Anastasio, A.R. Brady, A.E. Childress, I.V. Farr, N.T. Hancock, J. Lampi, L.D. Nghiem, M. Xie, N.Y. Yip, Standard methodology for evaluating membrane performance in osmotically driven membrane processes, Desalination 312 (2013) 31–38.
[25] A. Tiraferri, N.Y. Yip, W.A. Phillip, J.D. Schiffman, M. Elimelech, Relating performance of thin-film composite forward osmosis membranes to support layer formation and structure, J. Membr. Sci. 367(1–2) (2011) 340–352.
[26] A.P. Straub, N.Y. Yip, M. Elimelech, Raising the bar: Increased hydraulic pressure allows unprecedented high power densities in pressure-retarded osmosis, Environ. Sci. Technol. Lett. 1 (2014) 55–59.
[27] Y.C. Kim, Y. Kim, D. Oh, K.H. Lee, Experimental investigation of a spiral-wound pressure-retarded osmosis membrane module for osmotic power generation, Environ. Sci. Technol. 47(6) (2013) 2966–2973.
[28] S. Chou, R. Wang, A.G. Fane, Robust and High performance hollow fiber membranes for energy harvesting from salinity gradients by pressure retarded osmosis, J. Membr. Sci. 448 (2013) 44–54.
[29] HTI™ Hydration Technology Innovations: Forward Osmosis Membranes Technical Sheet, Model: HTI OsMem™ TFC-ES Membrane, 2014.
[30] A. Tamburini, P. Pitò, A. Cipollina, G. Micale, M. Ciofalo, A thermochromic liquid crystals image analysis technique to investigate temperature polarization in spacer-filled channels for membrane distillation, J. Membr. Sci. 447 (2013) 260–273.
[31] L. Gurreri, A. Tamburini, A. Cipollina, G. Micale, M. Ciofalo, CFD simulation of mass transfer phenomena in spacer filled channels for reverse electrodialysis applications, Chem. Eng. Trans. 32 (2013) 1879–1884.
[32] L. Gurreri, A. Tamburini, A. Cipollina, G. Micale, M. Ciofalo, CFD prediction of concentration polarization phenomena in spacer-filled channels for reverse electrodialysis, J. Membr. Sci. 468 (2014) 133–148.
[33] L. Gurreri, A. Tamburini, A. Cipollina, G. Micale, M. Ciofalo, Flow and mass transfer in spacer-filled channels for reverse electrodialysis: A CFD parametrical study, J. Membr. Sci. 497 (2015) 300–317.
[34] A. Tamburini, M. Renda, A. Cipollina, G. Micale, M. Ciofalo, Investigation of heat transfer in spacer-filled channels by experiments and direct numerical simulations, Int. J. Heat Mass Transfer 93 (2016) 1190–1205.